A Novel Design for Interferometer Based Dynamic Atomic Force Microscope

IISER Pune

HRISHIKESH INGOLE

Registration No: 20191193

Indian Institute of Science Education and Research, Pune

Thesis Supervisor: Dr Shivprasad Patil, IISER Pune

Thesis Expert: Dr Umakant Rapol, IISER Pune

May 15, 2024

This Work Is Dedicated To My Family

Certificate

This is to certify that this dissertation entitled "**A Novel Design for Interferometer Based Dynamic Atomic Force Microscope**" towards the partial fulfilment of the **BS-MS** dual degree programme at **the Indian Institute of Science Education and Research, Pune** represents study/work carried out by "**Ingole Hrishikesh Shivaji at IISER Pune**" under the supervision of "**Dr Shivprasad Patil, Professor, Department of Physics**" during the academic year **2023-24**

Sign of the Student
Ingole Hrishikesh Shivaji

Sign of the Supervisor
Dr Shivprasad Patil

Declaration

I hereby declare that the matter embodied in the report entitled "**A Novel Design for Interferometer Based Dynamic Atomic Force Microscope**" are the results of the work carried out by me at the **Department of Physics, IISER Pune**, under the supervision of **Dr Shivprasad Patil** and the same has not been submitted elsewhere for any other degree.

Sign of the Student
Ingole Hrishikesh Shivaji

Sign of the Supervisor
Dr Shivprasad Patil

Acknowledgements

I extend my sincere gratitude to Dr. Shivprasad Patil for his unwavering support and providing me with the invaluable opportunity to work in his lab. His kindness and encouragement have been instrumental in my growth.

To my family, I am deeply thankful for their love, care, and support throughout my journey.

A big shoutout to the entire LDAB parivar. Aniket, Ankit, Arindam, Mehul, Raghav, Rajit, Samarth, Sanket, Shubhankar, Varun, and Vedant. I've had a blast with you all and you've helped me grow. You gave me an environment where I could express myself without getting judged. Whether I was sick, depressed, anxious or stressed, you guys were always there to support me. I will always cherish the memories of the nights before the exams, the trips we went to and roaming around the city.

I am very grateful to my fellow lab members, Shatruhan, Ajith, Surya, Sujal, Vishal, Shrikrishna, Swarnao, and Mayank. Our conversations over chai were always filled with warmth and laughter, making the lab environment truly enjoyable.

Siddhi, you were an integral part of my college journey. I would always cherish the memories of the time we spent together. You made me a better person. Thank you so much for tolerating me all this while. Keep singing my favourite songs :)

Contents

1 Introduction 12

1.1 The History 13

2 Atomic Force Micrscopy Methods 18

2.1 Imaging Modes 18

2.1.1 Contact Mode 18

2.1.2 Tapping Mode 19

2.1.3 Non-contact mode 19

2.2 Dynamic AFM Methods 20

2.2.1 Amplitude Modulation AFM 20

2.2.2 Frequency Modulation AFM 20

2.3 Force Spectroscopy 20

2.4 Signal Detection Schemes 21

2.4.1 Optical Beam Deflection Detection 21

2.4.2 Other deflection measurement methods 21

2.5 Equation of Motion 22

2.5.1 Point Mass Model 22

2.5.2 Continuous Beam Model 26

2.6 Validity of Point Mass Model 30

2.7 Motivation of the Project 31

3 Methods 33

3.1 The Interferometer Based Atomic Force Microscope 33

3.1.1 Fiber Based Interferometer Setup 33

3.1.2 Optical-fiber: a partial reflective mirror 34

3.2 Approaching the substrate towards the cantilever 35

3.2.1 Coarse-motion with Hammer Piezo . . . 35
3.2.2 Fine-motion with Scanner Piezo . . . 36
3.3 The Need Of The New Design . . . 38
3.4 The New Design . . . 38
3.4.1 Cantilever Holder . . . 38
3.4.2 Five Axis Nano Positioner . . . 38
3.4.3 Sample Movement Assembly . . . 39
3.5 Assembly . . . 40
3.6 Calibration . . . 40
3.6.1 Fiber Piezo . . . 40
3.6.2 Scanner Piezo . . . 41

4 Results and Discussion **49**
4.1 Optical fiber and the cantilever . . . 49
4.2 Cantilever and the substrate . . . 50
4.3 Discussion . . . 51

5 Future Plans **52**

List of Figures

1.1 A schematic of AFM. Image adopted from wikipedia. 13
1.2 Early design of stylus profiler in 1920s with height resolution $\sim$ 25 nm. Figure Adopted from:[9] 14
1.3 Schematic of a scanning tunnelling microscope (STM). 15

2.1 Schematic of beam deflection detection system 21
2.2 A simplified diagram illustrating a cantilever, approximated as a point mass, experiencing a linear interaction force. (a) Depicts the scenario where the base, driven by $Ae^{i\omega t}$, induces point-mass approximation due to excitation. (b) Illustrates the scenario where the base is firmly held, and the tip is oscillated with a force $F_0e^{i\omega t}$. . 24
2.3 Diagram depicting a vibrating cantilever, acknowledging its continuous structure, subject to a linear interaction force. (a) Illustrating the scenario of a base-excited cantilever, with the base propelled by $Ae^{i\omega t}$. (b) Depicting the scenario of a tip-excited cantilever, where the base remains firmly fixed, and the tip is stimulated by force $F_0e^{i\omega t}$. 27

3.1 The diagram of the optical fiber-based interferometer arrangement employed to sense the displacement of the cantilever developed by Patil et al. (2005) [15]. In this interferometer-based detection method, the cantilever back serves as one of the mirrors within the Fabry-Perot etalon. The other mirror (semi-mirror being the TiO_2 coated cleaved end of the optical fiber) The displacement of the cantilever generates a corresponding signal in the photodiode. This signal from the photodiode quantifies the displacement (y) of the cantilever end. Figure adopted from: [8] 34
3.2 Scanner piezo electrode arrangement. 36

3.3 The current design of the interferometer based atomic force microscope developed by Dr Patil *et al* [15]. Here, you can see, when one needs to change the sample, one has to remove the cantilever holder as well as optical fiber setup. 37
3.4 Dimensions of Cantilever Holder. Note: The angle between the sides 35mm and 15mm is 12^0 39
3.5 Cantilver Holder with its components. Macor(5x5x2), Piezo(5x5x1), Cantilever Chip, Copper Plates 40
3.6 Cantilever Holder 41
3.7 Five Axis Nanopositioner along with cantilever holder assembly 42
3.8 Depiction of magnets holding the front and fiber plate. Thin sapphire glass sheets are glued on magneic steel plates where ruby balls touches the magnetic steel plate. Note that magnets are not touching the magnetic plates. This ensures that plates are only touching the ruby balls. 43
3.9 Directions of piezo movements and wlwctrical connections. Connections Z, H2, M, H1 correspond to base plate whereas, connections Zy, H2y, My, H1y correspond to front plate. 43
3.10 The X, Y, and Z axes 43
3.11 The Base Plate 44
3.12 The Base Plate 44
3.13 The Base Plate 44
3.14 The Front Plate 45
3.15 The fiber Plate 45
3.16 The sample movement assemply containing scanner piezo, hammer piezo, leaf spring, etc. 45
3.17 Assembly for the interferometer based AFM (view 2) 46
3.18 Assembly for the interferometer based AFM (view 3) 47
3.19 Assembly for the interferometer based AFM (view 1) 48

4.1 Fiber piezo voltage (V) Vs Time (min) for the five experiments performed. The changes in fiber piezo voltage indicate the drift between the end of the optical fiber and the cantilever. The drift between optical fiber and cantilever is found to be: Experiment 1: 292.672 nm, Experiment 2: 467.059 nm, Experiment 3: 192.000 nm, Experiment 4: 94.093 nm, Experiment 5: 23.232 nm 50

4.2 Avg Z voltage (V) (given to scanner piezo) Vs Time (min) for the five experiments performed. The changes in Z voltage indicate the drift between cantilever and the substrate. The drift between the cantilever and the substrate for 50 minutes was found to be: Experiment 1: 4.878 nm, Experiment 2 14.202 nm, Experiment 3: 1.206 nm, Experiment 4: 2.772 nm, Experiment 5: 1.242 nm 51

List of Tables

Abstract

Conventional AFMs measure cantilever bending, the home-built AFM, developed by Dr. Patil's group, measures cantilever displacement. This enhanced sensitivity, facilitated by the interferometer, enables precise measurements of extremely small amplitudes. Additionally, employing a stiffer cantilever operating in an off-resonance regime is advantageous for experiments conducted in a liquid environment, surpassing the capabilities of traditional AFMs utilised in protein-pulling experiments.

The home-built AFM's current iteration uses an optical fibre setup to construct a Fabry-Perot interferometer. A TiO_2 semi-mirror is coated to the end of a cleaved optical fibre, and when aligned parallel to the cantilever, it forms a Fabry-Perot cavity. However, aligning the optical fibre is challenging and time-consuming, often resulting in sample dehydration.

This project aims to devise a novel setup for our AFM to make this alignment procedure easier by making a new design for the home built AFM.

Chapter 1

Introduction

Atomic force microscopy (AFM) enables the observation and accurate measurement of surface features with unparalleled precision and detail. By employing AFM, we can capture images that unveil the positioning of atoms within a specimen and examine the structure of individual molecules, among other functionalities.

One of the significant advantages of AFM lies in its versatility to image a wide range of samples, whether they are rigid like ceramic materials, metallic nanoparticles, or soft substances such as polymers, cells, or DNA molecules. Additionally, beyond its conventional role as a microscope for imaging purposes, AFM offers various 'spectroscopic' modes enabling the measurement of other sample properties at the nanometer scale. Consequently, since its inception in the 1980s, AFM has found applications across various scientific disciplines including chemistry, biology, physics, materials science, nanotechnology, astronomy, and medicine. To analyze a wide range of samples, Governmental, academic, and industrial research facilities depend on AFM to deliver precise high-definition images.

AFM stands out from conventional microscopes as it does not rely on focusing light or electrons onto a surface, as optical or electron microscopes do. Instead, AFM employs a sharp probe to physically probe the sample's surface, generating a topographical map of its height. While this method lacks the two-dimensional projection of traditional imaging microscopes, the height data from AFM allows for straightforward measurement of feature height, length, width, or volume. Despite its unique operation, the treatment of AFM data to generate images is relatively simple

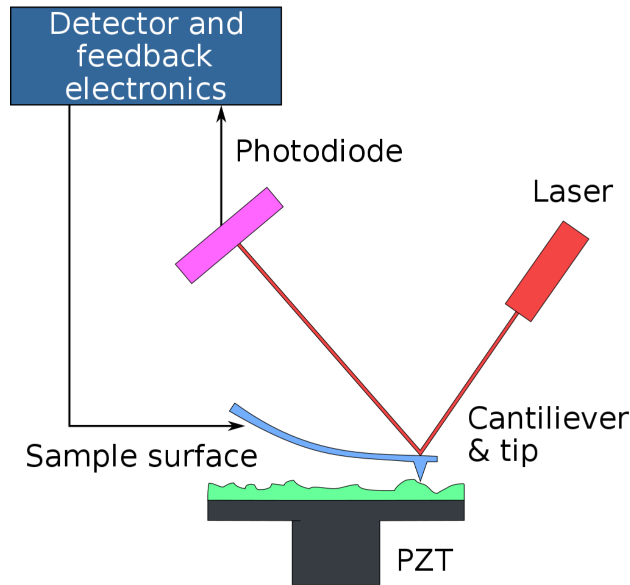

Figure 1.1: A schematic of AFM. Image adopted from wikipedia.

and flexible, enabling the observation of samples from various angles with basic analysis software.

Yet, the unique operation of AFM, involving physical interaction between the probe and the sample, renders it less intuitive to operate in comparison to optical microscopes. Unlike the familiar concepts of focusing, illumination, and depth of field in light microscopy, AFM operation lacks these elements, initially causing confusion for users. Nonetheless, understanding the underlying principles of AFM operation simplifies data analysis and acquisition, making the technique more intuitive over time. AFM, although built upon existing methods, marks a revolutionary advancement in microscopy.

1.1 The History

As noted earlier, the Atomic Force Microscope (AFM) functions by maneuvering a probe over the surface of a specimen, systematically generating a map that illustrates the surface topography. However, this method wasn't pioneered by the AFM; it has its roots in an earlier instrument known as the stylus profiler. The stylus profiler employed a sharp tip attached to a small rod, which was dragged along the sample surface to create a topograph. Stylus profiler, introduced by Shmalz in 1929 is shown in figure 1.2 [20]. The stylus profiler utilized an optical lever mechanism to track the motion of a sharp probe positioned at the tip of a cantilever. The stylus profiler was capable of generating an enlarged representation of the surface by documenting the movement of the stylus onto photosensitive paper. Such 'microscopes' generated profile 'images' with magnifications

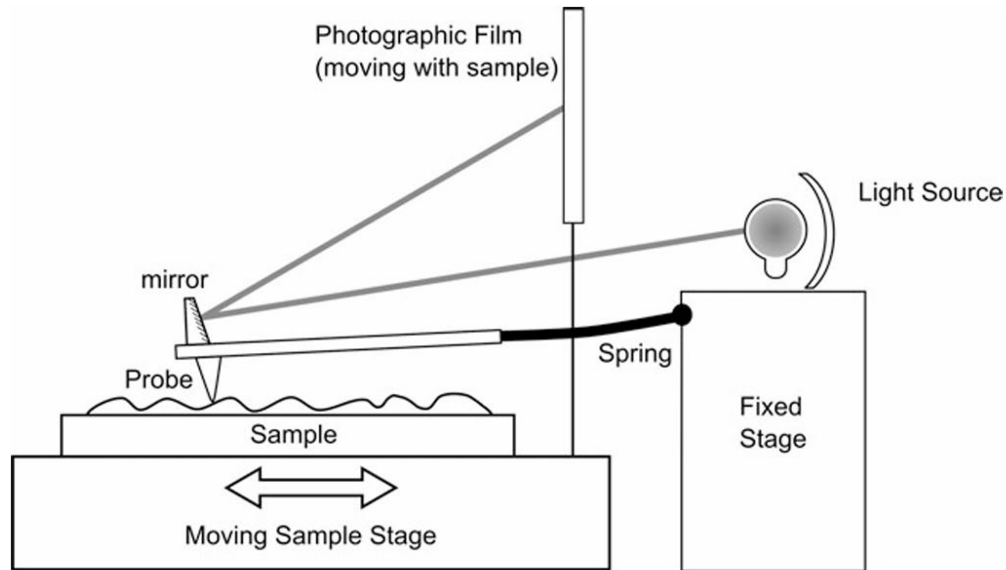

Figure 1.2: Early design of stylus profiler in 1920s with height resolution $\sim$ 25 nm. Figure Adopted from:[9]

exceeding 1000.

One prevalent drawback was the potential bending of the probe due to collisions with surface features. The phenomenon of 'probe bending' occurred due to lateral forces exerted on the probe upon encountering significant surface features. Becker proposed a solution to this issue in 1950 by suggesting the vibrating the tip (probe) [2]. He noted that the detail of the resulting images using this vibrating profile method would rely on the tip sharpness. Today, stylus profilers are much more sophisticated but inherent issues persist. Unregulated contact between the probe and the surface can result in damage to the probe when dealing with hard samples, or harm to the sample in the case of soft samples. In either scenario, the quality and attainable resolution of the resulting image would be compromised.

In 1971, Russell Young introduced a variation of the stylus profiler that operated without physical contact, known as the topografiner [21].Young utilized the relationship between the electron field emission current and the distance between a sharp metal tip and a surface for samples which are good conductors of electricity. In the topografiner, the tip was attached directly to a piezo, which controlled vertical movement (z) above the surface. Further, piezo allowed movement of the tip in other directions across the sample.

A feedback circuit with electron emission current as feedback parameter to control the movement

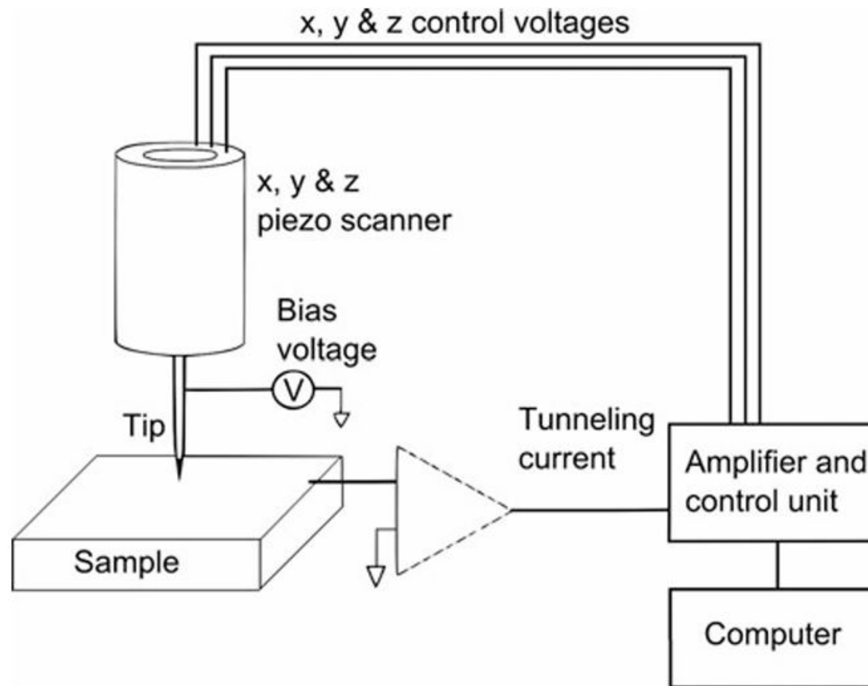

Figure 1.3: Schematic of a scanning tunnelling microscope (STM).

of the z-axis piezo, to maintain a fixed tip-sample distance. Subsequently, using the x and y piezoelectric ceramics, the tip scanned the surface in the X-Y plane. By monitoring the X,Y, and Z positions of the tip, a 3-D image of the surface was reconstructed. However, the resolution was limited by vibrations.

In 1981, Binnig *et al*, researchers at IBM, enhanced the vibration isolation of a device akin to the topografiner, enabling the monitoring of electron tunneling instead of field emission between the tip and the sample. This pioneering instrument marked the inception of the scanning tunneling microscope (STM) [6]. A schematic representation of the STM is depicted in Figure 1.3. A feedback loop maintians the tip sample distance, where the feedback parameter is tunneling current between tip and sample and the tip scans over the surface in X and Y directions.

Similar to the topografiner, three piezo control the x, y, and z motion of the tip across the surface. The z piezo manitains the tap sample distance and hence creates a topograph as tip traverses over the sample. The STM's remarkable has an upperhand over the topografiner due to electron tunneling's heightened sensitivity to the distance between tip and sample compared to field emissions.

In fact, electron tunneling probability is so profoundly influenced that the atom at the end of the tip is capable of tunneling effectively. Consequently, the tip's structure far from the surface holds

minimal significance, making it relatively straightforward to produce atomically sharp tips. Initially, Binnig and Rohrer resorted to magnetically levitating the entire instrument to counteract vibrations during their initial experiments; however, subsequent designs obviated this requirement. The outcomes of these early experiments were extraordinary; Binnig *et al* succeeded in visualizing individual silicon atoms on a surface [7]. Prior to the advent of the STM, achieving such resolution necessitated a transmission electron microscope (TEM), which weighs several tons also occupies considerable space.

Moreover, at the time of the STM's invention, atomic structures could only be indirectly observed via diffraction patterns, however the STM facilitated direct imaging of individual atoms. The STM's capability to achieve this feat as a compact instrument, suspended with springs to mitigate vibrations, appeared nothing short of remarkable. Consequently, Binnig and Rohrer were awarded the Nobel Prize in Physics in 1986 for their groundbreaking invention of the STM.

The scanning tunneling microscope (STM) represented a significant breakthrough in scientific research however, its applicability was limited to electrically conductive samples. Despite this constraint, the STM remains a valuable tool, particularly in physics and materials science, where it is extensively employed for characterizing the atomic and molecular arrangement of conductors and semiconductors.

However, the STM's restriction to conductive samples prompted its inventors to contemplate a new instrument capable of imaging insulating samples. In 1986, Binnig *et al* introduced the "Atomic Force Microscope" (AFM) [5]. In their seminal paper, they detailed the replacement of the wire probe in the STM with a lever consisting of a small diamond affixed meticulously to the end of a gold strip spring. This arrangement constituted the cantilever of the inaugural AFM.

The cantilever motion was controlled by measuring the tunneling current between the gold spring and a suspended wire positioned above it. This configuration exhibited high sensitivity to the probe's movement as it traversed across the sample, facilitated by piezos. Binnig et al. suggested in their paper that vibrating the cantilever above the surface could enhance the AFM's performance [4]. Fortunately, contemporary AFM techniques no longer necessitate the intricate process of attaching tiny diamonds to gold levers.

The invention of the AFM marked a pivotal moment, catalyzing a revolution in imaging capabilities. Suddenly, with a relatively inexpensive and straightforward instrument, it became feasible to

capture unprecedented resolution images of nearly every sample.

In the wake of the AFM's invention, the gold leaf/diamond configuration was supplanted by a significantly reliable method of cantilever production using silicon lithography [1]. This advancement facilitated the mass production of cantilevers. Additionally, it became evident that easier detection methods than those employed by the STM could be utilized to monitor the cantilever's movement. Presently, the majority of AFMs employ a beam deflection detection method, offering much more simplified setup compared to the STM.

Moreover, as proposed by Binnig et al., the incorporation of oscillating modes has reduced the risk of sample damage and samples of much more variety could be imaged.

Because of considerable interest in atomic force microscopy, commercial AFMs swiftly entered production, with the first models becoming available as early as 1988. AFM and STM are commonly grouped together under the umbrella term "scanning probe microscopy" (SPM).

As AFM and STM both have similar structure, constructing an instrument capable of performing functions of both of these types is relatively straightforward hence both STM and AFM, the techniques are often perceived as closely related. However, AFM has undergone significant modifications to enable the measurement of various properties and the execution of numerous non-imaging experiments. Coupled with its greater versatility of the types of samples that can be imaged, AFM has become more widely utilized than STM today.

Chapter 2

Atomic Force Micrscopy Methods

2.1 Imaging Modes

Using nature motion of the cantilever tip, operations of AFM are categorized into three modes: contact mode (also known as static mode), tapping mode, and non-contact mode.

The first AFM was operated in contact mode, which means, measuring static deflection of the probe. After one year, Martin, Williams, and Wickramasinghe were interested in measuring long range forces(3-15nm). They operated the AFM in dynamic mode, which means oscillating the probe sinuosoidally[13]. They noticed that the amplitude varied with the tip-surface distance and used amplitude as a feedback parameter to image the sample (popularly known as amplitude modulation or tapping mode AFM).

2.1.1 Contact Mode

In contact mode, the tip is dragged over the surface of the sample, and the surface topography is gauged by directly measuring the cantilever deflection or, more commonly, by monitoring the feedback signal needed to maintain the cantilever at a constant position. Since static signal measurement is susceptible to noise and drift, low stiffness cantilevers are utilized to obtain a substantial signal generated by deflection simultaneously minimizing force of interaction. The tip is kept at a distance where overall force is repulsive, if it is at a distant where attractive forces are dominant, then tip can snap directly to the surface.

2.1.2 Tapping Mode

In typical environmental conditions, most samples tend to have a meniscus, posing a challenge for contact mode AFM by causing the tip to adhere to the surface. To tackle this, tapping mode, was introduced. Tapping mode imaging is gentler than contact mode, reducing surface and tip damage due to shorter force application duration and lower horizontal forces.

In this mode, the cantilever oscillates up & down close to the resonance frequency. This oscillation can be induced by various means, such as a small piezo element, magnetic field, or laser based heatng. Generally the amplitude of oscillation ranges from several nanometers to 250 nanometers.

As the tip comes closer and closer to the sample surface, forces like van der Waals forces and electrostatic forces alter the cantilever's oscillation amplitude. This change in amplitude is given as a feedback parameter to the cantilever-sample separation same.

The phase difference between the cantilever's tip and the driving signal, provides information about energy dissipation and revealing contrast in materials with varying stiffness or adhesion properties.

2.1.3 Non-contact mode

In this mode, the cantilever tip oscillates above the sample surface without making physical contact. It oscillates close to its resonant frequency, with amplitudes generally ranging from a nanometers to picometers. The strongest forces, like van der Waals forces, act within a narrow range above the surface, causing a decrease in the cantilever's resonance frequency. A feedback loop maintain the mean separation between tip and sample to maintain constant oscillation amplitude or frequency. A computer programme construct a topograph of the surface.

Non-contact mode avoids tip and sample damage observed in contact mode, making it advantageous for delicate and biological samples. In dynamic mode operation, frequency modulation tracks the cantilever's resonance frequency, while amplitude modulation adjusts the cantilever excitation to a defined amplitude. Image formation involves plotting changes in tip position and recorded variables, with intensity corresponding to hue, typically shown on a color scale.

2.2 Dynamic AFM Methods

There are mainly two dynamic AFM methods: Amplitude Modulation (AM AFM) and Frequency Modulation (FM AFM).

2.2.1 Amplitude Modulation AFM

In amplitude modulation AFM,the tip, undergoes oscillation when it is close to the sample surface. The tip is oscillated on or near its resonance frequency. Forces of interaction between tip-surface cause a decrease in the oscillation's amplitude compared to its free amplitude value. Experimental parameters in amplitude modulation AFM include the oscillation amplitude and the phase difference between the driving signal and tip movement. The amplitude serves as a feedback parameter to delineate surface topography. The resultant force exerted by the tip on the sample surface, at the tip-surface interface, is influenced by various factors including the initial amplitude, tip radius, etc.

2.2.2 Frequency Modulation AFM

In this method the feedback parameter entails a change in frequency between the resonant frequency when tip away from the surface and the resonant frequency when the tip is in the proximity of the surface. This resonant frequency is influenced by the tip-surface interaction forces. The spatial variation of the frequency shift, provides contrast and surface topography is profiled to create an image with a consistent frequency shift.

2.3 Force Spectroscopy

Besides its imaging capabilities, AFM is widely used for force spectroscopy, allowing for the direct measurement of interaction forces between the tip and sample as their separation varies. This measurement produces a force versus extension plot. In force spectroscopy, the tip is approached and withdrawn from the sample while monitoring the cantilever's deflection in response to piezoelectric displacement. Such measurements have been instrumental in studying various phenomena, like molecular bonding, Van der Waals forces, and single molecule stretching and rupture forces, etc. Modern AFM setups can routinely detect forces on the order of a few piconewtons. Force spectroscopy can be conducted in static as well as dynamic modes.

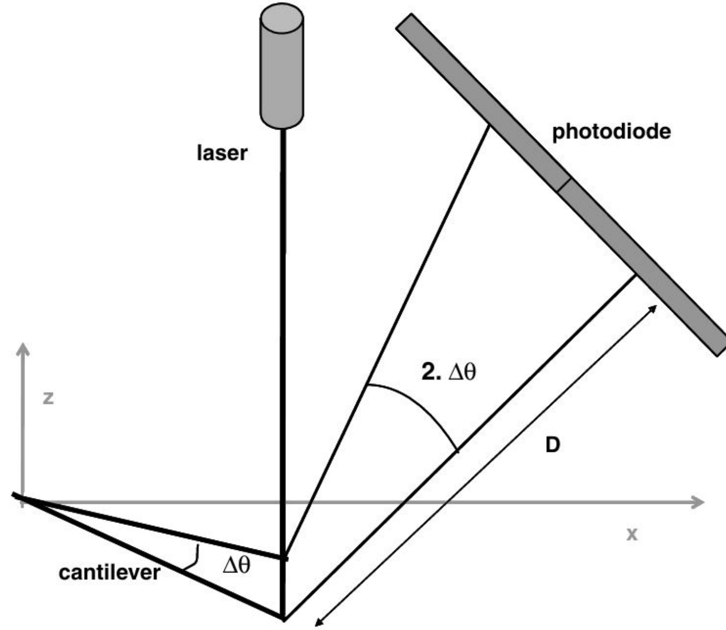

Figure 2.1: Schematic of beam deflection detection system

2.4 Signal Detection Schemes

2.4.1 Optical Beam Deflection Detection

This is the most popular signal detection scheme, owing to its simplicity and commercial availability. This scheme of detection is one of the main reasons for quick success of AFM. A light beam coming from a laser is reflected at the back of the cantilever to a four quadrant photodiode. The photo-diode measures the deflection of cantilever and gives an output signal. The schematic of beam deflection detection is shown in figure 2.1. The four quadrant photo-diodes enables the detection of both vertical as well as horizontal forces. This method doesn't measure vertical displacement(z) directly, it measures the bending(slope: dy/dx) of the cantilever. Euler Bernoulli theory can be applied to study cantilever dynamics (see section 2.5).

2.4.2 Other deflection measurement methods

Piezo-electric detection[11], Laser Doppler vibrometry[14], Optical interferometry[19][15], capacitive detection[12], etc. are less oftenly used deflection detection schemes.

2.5 Equation of Motion

Euler-Bernoulli equation can be used to study bending of homogeneous rectangular cantilever beam in viscous medium where internal damping of cantilever beam has been ignored:

$$-\tilde{\rho}\tilde{S}\frac{\partial^2 y(x,t)}{\partial t^2} - \gamma_c \frac{\partial y(x,t)}{\partial t} = EI\frac{\partial^4 y(x,t)}{\partial x^4} \tag{2.1}$$

where

x: co-ordinate along the cantilever length(X-axis) with x = 0 at the clamped end and x = L at the free end.

y: the displacement along the perpendiclar direction of cantilever (Y-axis)

$\tilde{\rho}\tilde{S} = \rho S + m_a$, m_a is hydrodynamic added mass, ρ is is mass density of cantilever material, S is the cross sectional area of cantilever perpendicular to its length

γ_c: The cantilever drag coefficient per unit length

E: Young's modulus

$I = \frac{bh^2}{12}$: second area moment

2.5.1 Point Mass Model

Variable separation method is used to solve 2.1. For the space part, the boundary co

Let's assume,

$$y(x,t) = y(x)Y(t) \tag{2.2}$$

substituting 2.2 into 2.1, and dividing entire equation by $y(x)Y(t)$, we get:

$$\frac{1}{y^4}\frac{d^4 y}{dx^4} = -\frac{\tilde{\rho}\tilde{S}}{EIY(t)}\frac{\partial^2 Y(t)}{\partial t^2} - \frac{\gamma_c}{EIY(t)}\frac{\partial Y(t)}{\partial t} \tag{2.3}$$

In 4.2, LHS is function of only x and RHS is function of only t. These two sides will be equal when when each of them will be equal to a constant, say k^4. So, we can write:

$$\frac{d^4y}{dx^4} = k^4 y(x) \tag{2.4}$$

and

$$\frac{d^2Y(t)}{dt^2} + \frac{\gamma_c}{\tilde{\rho}\tilde{S}}\frac{dY(t)}{dt} = -k^4\frac{EI}{\tilde{\rho}\tilde{S}}Y(t) \tag{2.5}$$

The general solution of 4.1 is given as:

$$y(x) = asin(kx) + bcos(kx) + csinh(kx) + dcosh(kx) \tag{2.6}$$

Where, constants a, b, c, d can be obtained by using following boundary conditions:

$$y(0) = 0, \qquad y'(0) = 0, \qquad y"(L) = 0, \qquad y'''(L) = 0 \tag{2.7}$$

After solving for these boundary conditions, (for detailed derivation, see: [17])

For the fundamental mode the equation of motion:

$$m^*\frac{\partial^2 w(t)}{\partial t^2} + \gamma_c L\frac{\partial w}{\partial t} + k_c w(t) = 0 \tag{2.8}$$

Where,

w : displacement of the point mass(fundamental mode)

$m^* = 0.2425m_c$: is effective cantilever mass

Using the fact that fundamental mode dominates over all the other modes as the force constant(k_1) of this mode almost equivalent to the static force constant(k_s) of the cantilever($k_1 = 1.030k_s$) hence, contribution from higher modes can be neglected. [10].

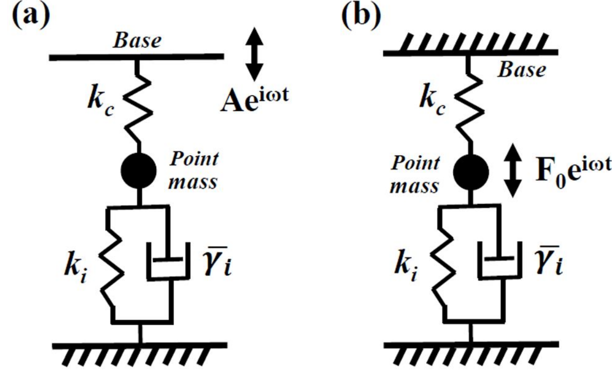

Figure 2.2: A simplified diagram illustrating a cantilever, approximated as a point mass, experiencing a linear interaction force. (a) Depicts the scenario where the base, driven by $Ae^{i\omega t}$, induces point-mass approximation due to excitation. (b) Illustrates the scenario where the base is firmly held, and the tip is oscillated with a force $F_0e^{i\omega t}$.

From equation 2.8, we understand that the equation of freely vibrating cantilever is the equation of a *damped harmonic oscillator*.

2.5.1.1 Base Excitation of Cantilever

In the PM model, when the cantilever base is excited sinusoidally with amplitude $Ae^{i\omega t}$, the tip experiences the force, $F_i = k_i w(t) + \bar{\gamma}_i \frac{dw(t)}{dt}$ (see Figure 2.2) We assume that this interaction force is linear visco-elastic.

The equation of motion for the PM can be given by:

$$m^* \frac{\partial^2 w(t)}{\partial t^2} + \gamma_c L \frac{\partial w(t)}{\partial t} + k_c(w(t) - Ae^{i\omega t)} - F_i = 0 \tag{2.9}$$

putting the value of F_i:

$$m^* \frac{\partial^2 w(t)}{\partial t^2} + \gamma' \frac{\partial w(t)}{\partial t} + k' w(t) = k_c A e^{i\omega t} \tag{2.10}$$

where:

$k' = k_c + k_i$ is effective stiffness

$\gamma' = \gamma_c L + \bar{\gamma}_i$ is effective damping coefficient

$k_c A$ is effective drive force

The amplitude(R_{pm})) and phase difference between base and tip (θ_{pm}) is given as:

$$R_{pm} = \frac{k_c A}{\sqrt{(k' - m^*\omega^2)^2 + (\omega\gamma')^2}}, \qquad \theta_{pm} = tan^{-1}(\frac{\omega\gamma'}{k' - m^*\omega^2}) \tag{2.11}$$

Eqn.2.11 can be further solved for k_i and γ' with using a condition: $\omega << \omega_0$:

$$k_i = k_c \left(\frac{Acos(\theta_{pm})}{R_{pm}} - 1 \right) \tag{2.12}$$

$$\gamma' = -\frac{k_c Asin(\theta_{pm})}{R_{pm}\omega} \tag{2.13}$$

where the assumptions are:

1. $\omega \ll \omega_0$ i.e. we are oscillating cantilever off-resonance, much below its resonance frequency

2. $F_i = k_i w(t) + \bar{\gamma}_i \frac{dw(t)}{dt}$ is considered as a linear perturbation

2.5.1.2 Tip Excitation

When tip excitation is performed with force ($F_0 e^{i\omega t}$), the net force on tip When the cantilever is excited from the tip can be treated as small perturbation due to a linear viscoelastic force

$$F_i = k_i w(t) + \bar{\gamma}_i \frac{dw}{dt}$$

, it can be treated as a PM, connected to a spring without mass, which is oscillated sinusoidally (see Figure 2.2(b)). For this PM, the Equation of motion can be given as:

$$m^* \frac{\partial^2 w(t)}{\partial t} + \gamma_c L \frac{\partial w(t)}{\partial t} + k_c w(t) - F_0 e^{i\omega t} = F_i \tag{2.14}$$

Equation 2.14 can be written as:

$$m^* \frac{\partial^2 w(t)}{\partial t} + \gamma' \frac{\partial w(t)}{\partial t} + k' w(t) = F_0 e^{i\omega t} \tag{2.15}$$

Equation 2.15 is an equation of motion of a forced damped harmonic oscillator with net stiffness $k' = k_c + k_i$, net damping $\gamma' = \gamma_c L \bar{\gamma}_i$. The amplitude R_{pm} and phase θ_{pm}, phase shift between drive and tip) of the tip will be expressed as:

$$R_{pm} = \frac{k_c A_0}{\sqrt{(k' - m^* \omega^2)^2 + (\omega \gamma')^2}} \tag{2.16}$$

$$\theta_{pm} = \tan^{-1} \left(\frac{A_0 \cos(\theta_{pm'})}{R_{pm'}} - 1 \right) \tag{2.17}$$

Again, this solution is valid when stiff cantilever (interaction force F_i is considered as the perturbation) is used and oscillated at off-resonance ($\omega << \omega_0$) with small-amplitude $F_i = k_i w(t) + \bar{\gamma}_i \frac{dw}{dt}$

2.5.2 Continuous Beam Model

In this model, the cantilever is treated as a continuous beam. Interaction force is considered as linear perturbation(i.e. $k_i << k_c$) where the interaction force is given by: $F_i = k_i w(t) + \bar{\gamma}_i \frac{dw(t)}{dt}$ and the oscillation frequency is much less than the resonance frequency (i.e. $\omega_0 << \omega$ and Eqn.2.1 is solved.

2.5.2.1 Base Excitation

When the cantilever is excited from base, following boundary conditions are applied(For detalied derivation, see: [17])

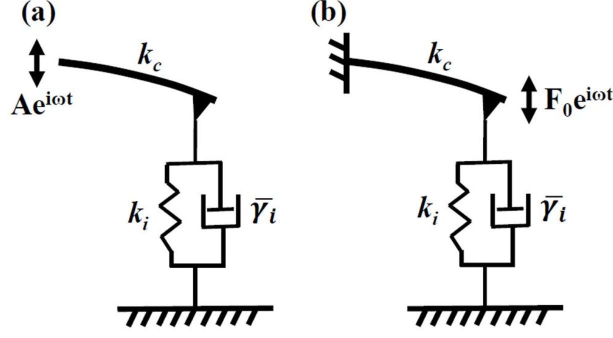

Figure 2.3: Diagram depicting a vibrating cantilever, acknowledging its continuous structure, subject to a linear interaction force. (a) Illustrating the scenario of a base-excited cantilever, with the base propelled by $Ae^{i\omega t}$. (b) Depicting the scenario of a tip-excited cantilever, where the base remains firmly fixed, and the tip is stimulated by force $F_0e^{i\omega t}$.

$$y(0) - A = 0, \qquad y'(0) = 0, \qquad y"(0) = 0, \qquad EIy'''(L) - (k_i - i\omega\bar{\gamma_i})y(L) = 0 \tag{2.18}$$

where

$$q = \frac{k_i + i\omega\bar{\gamma}_i}{EIk^3}$$

After solving, we get:

$$y(L) = A - \frac{gA}{3} + \frac{Az^4}{8} \tag{2.19}$$

$$y'(L) = \frac{-Ag}{2L} + \frac{Az^4}{6L} \tag{2.20}$$

where:

$$z = kL = \left[\frac{3(\tilde{\rho}\tilde{S}\omega^2 L - i\omega\gamma_c L)}{k_c}\right]^{\frac{1}{4}} << 1 \tag{2.21}$$

and

$$g = q(kL)^3 = \frac{3(k_i + i\omega\bar{\gamma_i})}{k_c} << 1 \tag{2.22}$$

In Eqn.2.21, the condition $z << 1$ ensures that excitation frequency is much small as compared to the resonance frequeny($\omega_0 << \omega$) and Eqn.2.22, the assumption $g << 1$ ensures that the stiffness of the cantilever is much larger than stiffness of the interaction ($k_i << k_c$).

After putting back the values of g and z, we get:

$$y(L) = \frac{A}{k_c}(k_c - k_i) - i\frac{A\omega}{k_c}\bar{\gamma_i} \tag{2.23}$$

and

$$\left.\frac{\partial y}{\partial x}\right|_{x=L} = \frac{A}{2k_cL}(-3k_i + \tilde{\rho}\tilde{S}\omega^2 L) - i(\frac{A\omega}{2k_cL}(3\bar{\gamma_i} + \gamma_c L) \tag{2.24}$$

Modulus of Eqn.2.24 gives us the amplitude of the slope at $x = L$ and the argument gives us the phase lag:

$$R_b = \frac{A}{2k_cL}\sqrt{(k_c - k_i)^2 + \omega^2\bar{\gamma_i^2}}, \qquad \theta_b = arctan\left(-\omega\frac{\bar{\gamma_i}}{k_c - k_i}\right) \tag{2.25}$$

Now, the real part as well as imaginary parts of bending(slope) can be calculated as:

$$X_b = \frac{3A_0}{K_cL}(K_c - K_i), \qquad Y_b = -\frac{3A_0\omega}{2K_cL}\bar{\gamma_i} \tag{2.26}$$

This is exactly same as the results by Benedetti *et al* [3]. The amplitude as well as phase for displacement y in the limit $g << 1$ and $z << 1$ are:

$$R_d = \frac{A_0}{k_c}\sqrt{(k_c - k_i)^2 + \omega^2\bar{\gamma_i}^2}, \qquad \theta_b = arctan\left(-\omega\frac{\bar{\gamma_i}}{k_c - k_i}\right) \tag{2.27}$$

The real part and imaginary part of y can be calculated as:

$$X_d = \frac{A_0}{k_c}(k_c - k_i), \qquad Y_d = -\frac{A_0\omega}{k_c}\bar{\gamma_i} \tag{2.28}$$

Here, subscript d stands for displacement.

Displacement Detection:

$$k_i = k_c\left(1 - \frac{X_d}{A}\right) \tag{2.29}$$

$$\bar{\gamma_i} = \frac{k_c Y_d}{A\omega} \tag{2.30}$$

Here, note that, the base amplitude is equal to cantilever's free amplitude($A \approx A_0$).

Slope Detection:

$$k_i = \frac{1}{3}\tilde{\rho}\tilde{S}\omega^2 L - \left(\frac{2k_c L}{3A}\right)X_b \tag{2.31}$$

$$\bar{\gamma_i} = \left(\frac{2k_c L}{3A\omega}\right)Y_b - \frac{\gamma_c L}{3} \tag{2.32}$$

2.5.2.2 Tip Excitation

When a cantilever is actuated from its tip and encounters a linear viscoelastic force due to the tethered macromolecule, the boundary conditions are specified by:

$$y(0) = 0, \qquad y'(0) = 0, \qquad y"(L) = 0, \qquad EIy'''(L) = (k_i + i\omega\bar{\gamma_i})y(L) - F_0 \tag{2.33}$$

Where $F_0 = kcA_0$ is the magnitude of externally applied force at the tip. A_0 is amplitude far away from the surface (free amplitude). After solving for these boundary conditions and taking taylor expansion for $z << 1$ and $g << 1$, we get(for detailed derivation, see: [17]):

Displacement Detection:

$$k_i = k_c\left(1 - \frac{X_d}{A}\right) \qquad and \qquad \bar{\gamma_i} = -\frac{k_c Y_d}{A\omega} \tag{2.34}$$

Slope Detection:

$$k_i = k_c\left(1 - \frac{2L}{3A}X_d\right) \qquad and \qquad \bar{\gamma_i} = -\frac{2k_c L}{3A\omega}Y_d \tag{2.35}$$

Summary:

Model	Excitation	Stiffness	Friction
CB(bending)	Base	$k_i = \frac{1}{3}\tilde{\rho}\tilde{S}\omega^2 L - \left(\frac{2k_c L}{3A}\right) X_b$	$\bar{\gamma_i} = \left(\frac{2k_c L}{3A\omega}\right) Y_b - \frac{\gamma_c L}{3}$
	Tip	$k_i = kc\left(1 - \frac{2L}{3A_0}X_b\right)$	$\bar{\gamma_i} = -\frac{2k_c L}{3A_0\omega}Y_b$
CB(Displacement)	Base	$k_i = k_c\left(1 - \frac{X_d}{A}\right)$	$\bar{\gamma_i} = \frac{k_c Y_d}{A\omega}$
	Tip	$k_i = k_c\left(1 - \frac{X_d}{A}\right)$	$\bar{\gamma_i} = \frac{k_c Y_d}{A\omega}$
PM	Base	$k_i = k_c\left(\frac{Acos(\theta_{pm})}{R_{pm}} - 1\right)$	$\gamma' = -\frac{k_c Asin(\theta_{pm})}{R_{pm}\omega}$
	Tip	$k_i = k_c\left(\frac{Acos(\theta_{pm})}{R_{pm}} - 1\right)$	$\gamma' = -\frac{k_c Asin(\theta_{pm})}{R_{pm}\omega}$

2.6 Validity of Point Mass Model

PM model has been used widely mainly because it makes of cantilever dynamic very simple to understand and its analytical solution is simple and direct.

Benedetti et al [3] raised doubts on experiments carried on nano-scale systems which use base excitation, slope detection and PM model.

The relaibility of the results depends on the accuracy of the mathematical model apllied, which is PM model. A detailed study performed by Rajput et al [16] shows that PM model predicts same results as CB model for base excited and tip excited dynamic AFM experiments when they are performed with following essential conditions:

1. Truly off resonance regime
2. Small tip amplitude
3. Stiff cantilevers

To quantify nano-scale viscocity without any artifacts, there ought to be absence of offset in initial phase. This can be achieved by using displacement-detection for base-excitation measurements and slope-detection for tip-excitation measurements[17].

AFM developed by Patil *et al* [15] meets all of the above mentioned conditions.

2.7 Motivation of the Project

The AFM developed by Patil *et al* [15] uses optical fiber based interferometer for detection of cantilever displacement. A cleaved end of the optical fiber is coated with TiO_2 forms a partially reflective mirror. The back of the gold coated cantilever acts as a fully reflective mirror. These two mirrors when aligned exactly parallel to each other, form a fabry-perot cavity. Due to high stiffness of cantilever and operating in frequency regime, much much smaller than its resonance frequency, it makes this AFM ideal for visco-elastic measurements. As the cantilever displaces, the distance between two mirrors change and hence the intensity of the fringe pattern. By studying the intensity pattern, one can calculte the displacement of the cantilever.

Despite its scientific capability, the instrument is difficult to use. Aligning the two mirrors exactly parallel to each other is a tedious and time consuming job. It often takes 1 to 2 hours to do this job. During this time the sample often dries out. The functionalised cantilever also oftenly dries out. Even if someone has to change the sample, the alignment is completely disturbed and one has

to begin back from scratch. Despite having an uperhand in measurements, as mentioned in section 2.6, the throughput is very low for this AFM.

This project aims to implement a new design for the interferometer based AFM to tackle the above mentioned issues.

Chapter 3

Methods

3.1 The Interferometer Based Atomic Force Microscope

3.1.1 Fiber Based Interferometer Setup

Dr Patil *et al* developed a novel interferometer based AFM [15]. Optical fiber is cleaved exactly perpendicular to its axis. This end is then coated with TiO_2, which acts as a partially reflective mirror. The cantilever back is gold coated, acting as a fully reflective mirror. Fiber end (partially reflective mirror is aligned parallel to the cantilever back by using a five axis nano-positioner. The cavity between parallely aligned mirror and cantilever acts as a fabry-perot cavity. An infrared laser (wavelength $= 1310$ nm) is sent through the optical fiber. Part of the laser reflects back from the end of the fiber depending on its reflectively and remnant of the laser falls on the cantilever back which also reflect back to the fiber. The two reflected lights interfere with each-other and it is allowed to fall on a photo-diode, kept at a fixed distance, which produces current. The output current is constant when the distance between mirrors is fixed. fiber position is moved back and forth with the help of fiber-piezo to get the interference pattern at the photo-diode. Software finds the position at which change in the output current is maximum. This position is known as quadrature-point. Slope of the pattern at quadrature point is the sensitivity of the interferometer. The position of the fiber is fixed at the maximum sensitivity which is determined by a software. fiber position is moved back and forth with the help of fiber-piezo to get the interference pattern at the photo-diode. Software finds the position at which change in the output current is maximum. This position is known as quadrature-point. Slope of the pattern at quadrature point is the sensi-

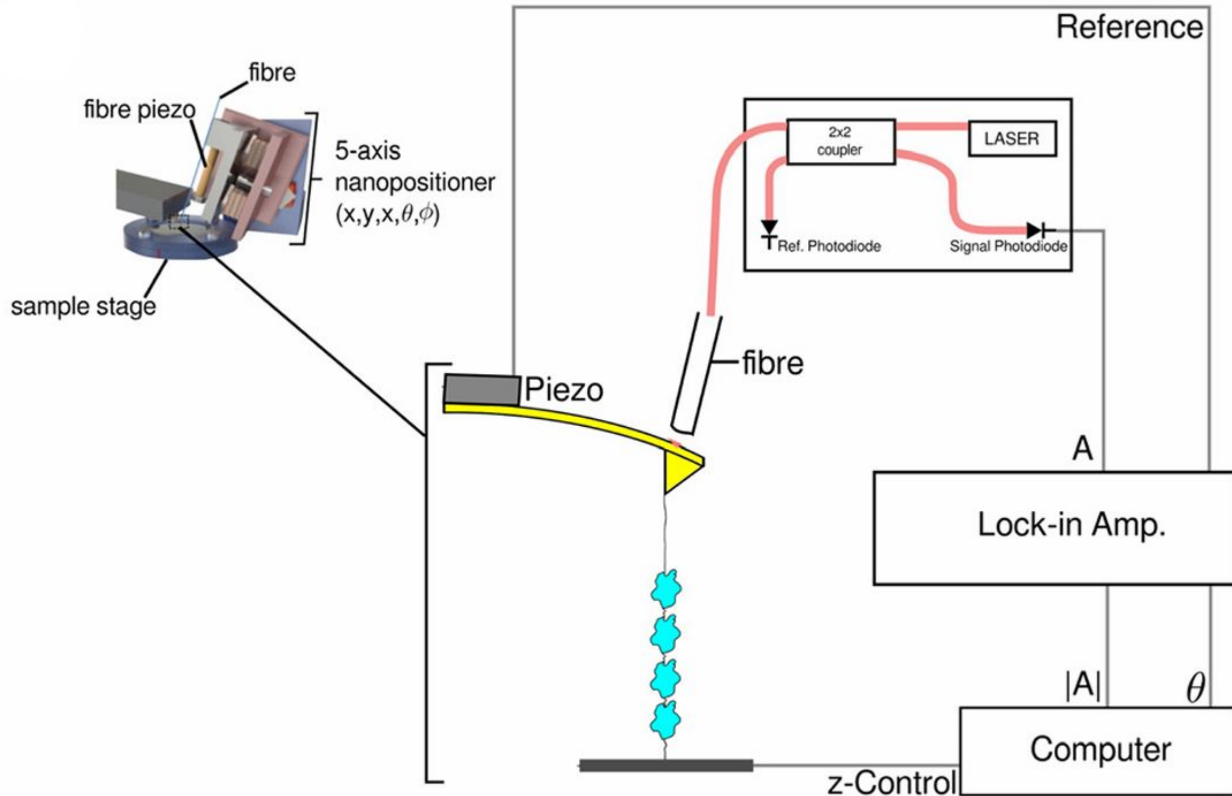

Figure 3.1: The diagram of the optical fiber-based interferometer arrangement employed to sense the displacement of the cantilever developed by Patil et al. (2005) [15]. In this interferometer-based detection method, the cantilever back serves as one of the mirrors within the Fabry-Perot etalon. The other mirror (semi-mirror being the TiO_2 coated cleaved end of the optical fiber) The displacement of the cantilever generates a corresponding signal in the photodiode. This signal from the photodiode quantifies the displacement (y) of the cantilever end. Figure adopted from: [8]

tivity of the interferometer. The interaction between tip & sample causes the distance variation between the mirrors which changes the output of the photo-diode. The change in the generated signal current is proportional to the displacement of the cantilever.

3.1.2 Optical-fiber: a partial reflective mirror

Transforming the fiber end into a partially reflective surface is a critical step in the interferometric detection system, as it serves as one of the mirrors in the Fabry-Perot etalon. Utilizing an optical fiber with a 9µm diameter core, we begin by flattening and partially reflecting its end through precise cleaving. The reflectivity of the cleaved end ranges around 2-3%. Subsequently, it undergoes immersion in a metal-organic precursor solution prepared by dissolving Titanium-(IV)-ethylhexoxide in p-xylene with a 1:2 weight ratio. Following this, the fiber end is exposed to the

blue flame of a Butane torch, burning away the organic compounds and leaving behind a uniform thin layer of metallic TiO_2. This process enhances the reflectivity of the fiber end to approximately 25%. Finally, the fiber is affixed onto the fiber-piezo for subsequent measurements.

3.2 Approaching the substrate towards the cantilever

The approaching of the substrate towards the cantilever is achieved though a LABVIEW programme.

Step 1: Scanner piezo is given a ramp Z voltage from +150V to -150V. At +150V, it is fully retracted and at -150V, it is fully extended. During this scanning, the lock-in amplifier records the amplitude of the tip of the cantilever and phase difference between the tip and the base of the cantilever. The amplitude of the tip drops as we approach closer and closer to the surface because of various interaction forces such as Van der Waal's force, tip-surface interaction force, etc. If the amplitude of the tip of cantilever drops to a specified value or setpoint. The programme is stopped. The scanner piezo retracts for safety reasons.

Step 2: If the amplitude doesn't drop to the specified value, then a set of saw-tooth like pulses are given to hammer piezo, which moves the substrate towards the cantilever and then step 1 is followed.

3.2.1 Coarse-motion with Hammer Piezo

A steel weight is attached to the bottom end of the hammer piezo to achieve inertial sliding. The top end of the hammer piezo is attached to a part which connects to the glass tube as well as scanner piezo, such that all three are concentric (see figure 3.16). The glass tube is held in the slot against gravity by pressing it with a leaf spring. The friction which holds the tube in place can be controlled by tightening/loosening the leaf-spring screws. The glass tube can be moved up or down if enough force is provided to overcome the friction. We use an inertial sliding mechanism to move the glass tube. The inertial sliding is achieved by using the "Hammer piezo". This will be used for coarse movement of the tip. The inertial sliding motion for the coarse movement of the tip is made in the following way. The hammer piezo is given a series of saw-tooth-like pulses. As the voltage provided to hammer piezo exponentially increases from to t_2, the piezo expands from length; L to L'. The bottom end of the piezo is free during this expansion. So, this end moves down. At t_2, the voltage is suddenly dropped to 0. This makes the piezo contract back to its original length; L. The steel weight being heavy makes the bottom end of the hammer piezo with more inertia. So

during the contraction, the sample platform is brought down while the steel weight stays stationary due to its larger inertia. The motion can be reversed by giving a negative pulse. Depending on the number of these pulses, pulse height, frequency, and friction on the sliding the movement can be controlled. Typical pulse width is 1 μ s and height is 30 V to 130 V. With a typical pulse, 50 nm to 100 μm steps are possible.

3.2.2 Fine-motion with Scanner Piezo

The scanner piezo is a tube piezo with four outer and one inner electrodes(EBL #2, gold over copper electrodes). The dimension of the tube is 0.256" x 0.020" x 1.181". Electrode arrangement is as shown in figure 3.2.

Fine motion along x,y, and z-directions are possible with this piezo. For z-motion, a voltage(V_z) is provided to all four outer electrodes while inner one is grounded. The pair of electrodes along the x direction receives equal and opposite voltage(V_x) to move along the x-direction. Similarly, the pair of electrodes along y-direction receive equal and opposite voltage; V_y. Each of the voltages ($Vz+Vx, Vz+Vy, Vz+Vx, Vz+Vy$) given to scanner piezo is between-150 V to 150 V. First; a voltage is-10 to 10 V range is made with a DAQ card or other circuits then it is amplified with PA88 opamps. The amplification is done with a gain of 7 or 15. Independent PA88 op-amps are used to amplify individual voltages.

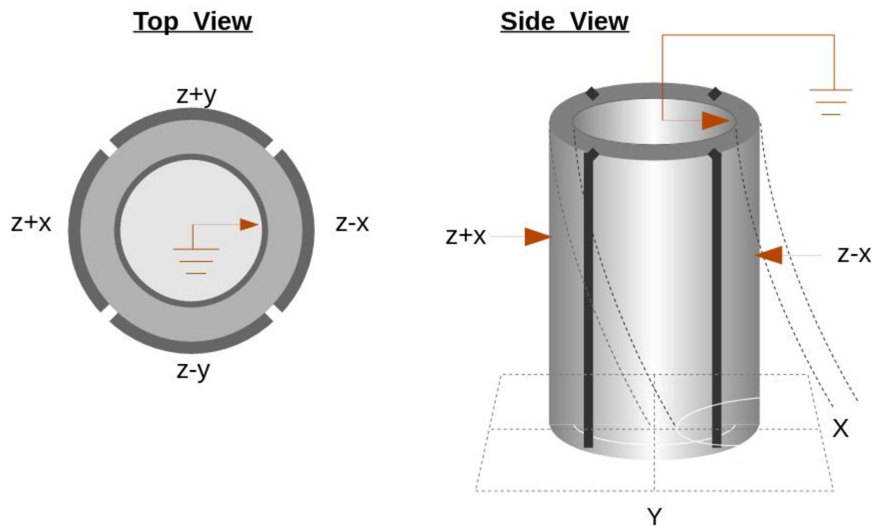

Figure 3.2: Scanner piezo electrode arrangement.

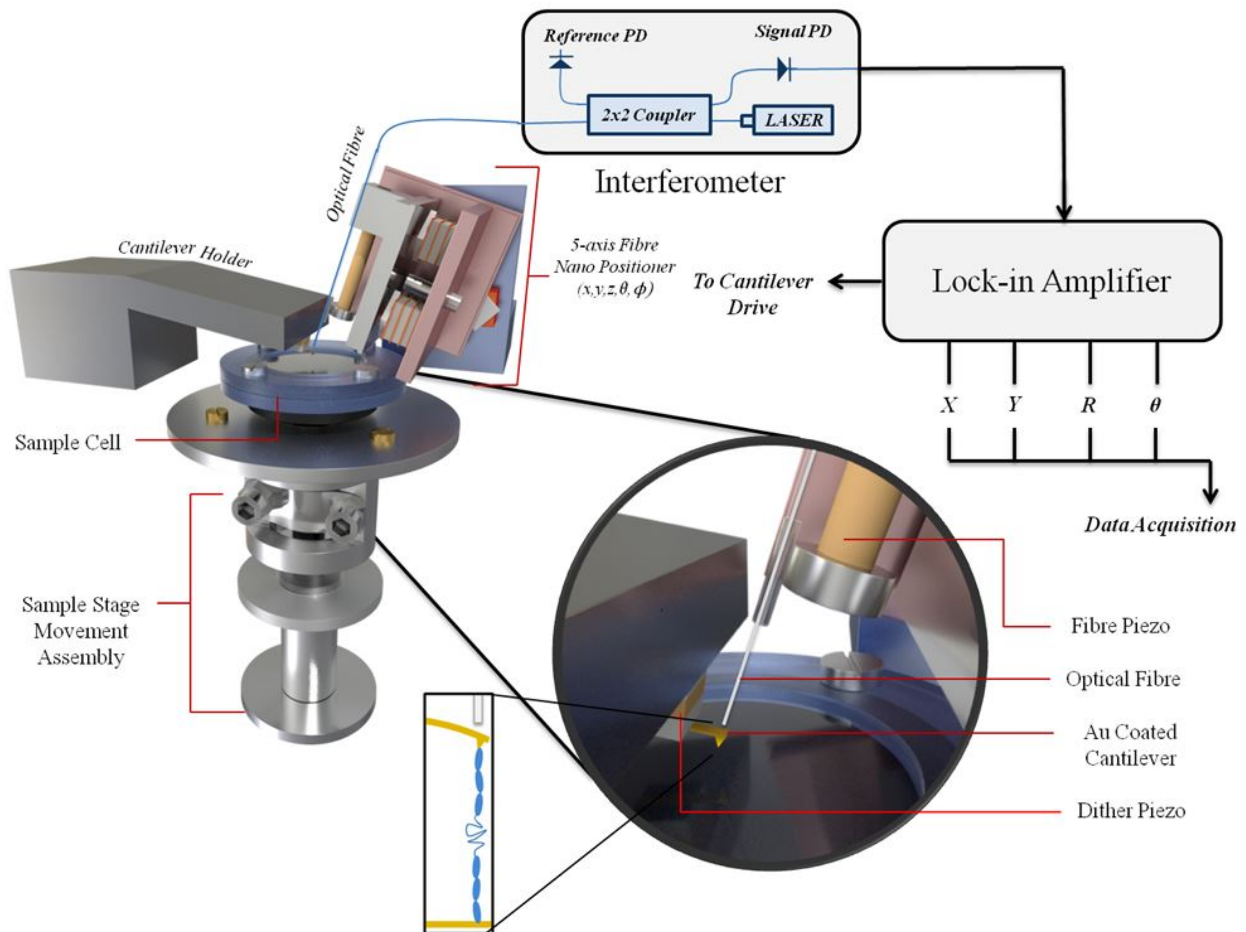

Figure 3.3: The current design of the interferometer based atomic force microscope developed by Dr Patil *et al* [15]. Here, you can see, when one needs to change the sample, one has to remove the cantilever holder as well as optical fiber setup.

3.3 The Need Of The New Design

Figure 3.3 depicts the current interferometer based setup developed by Dr Patil *et al* [15]. To detect the cantilever displacement, the coated end of the optical fiber has to be aligned parallel to the back of the cantilever. The semi mirror at the end of the optical fiber acts as a semi mirror, whereas the gold coated back of the cantilever acts as a fully reflecting mirror. The cavity between these two parallel mirror acts as a fabry perot cavity. The alignment procedure is tedious and time consuming. Often the sample dries out, the functionalized cantilever dries out, etc are the main challenges while operating this AFM. As you can see in figure 3.3, when one has to change the sample, the optical fiber setup and the cantilver holder has to be displaced, and hence the alignment process has to be done once again from scratch.

3.4 The New Design

For designing the components of AFM, SOLIDWORKS, an AUTOCAD based platform was used.

To tackle the issue mentioned in section 3.3, the optical fiber setup is being placed on the cantilever holder and this assembly has been placed on a rotating plate(see figure 3.18 and figure 3.19), so that when one has to change the sample, one can simply lift-rotate the plate, change the sample and perform the experiment with minimal re-alignment of the optical fiber. The rest design is exactly the same as previous iteration.

3.4.1 Cantilever Holder

This part holds the cantilever chip. The piezo is used to oscillate the cantilever for the dynamic mode force spectroscopy.

3.4.2 Five Axis Nano Positioner

The five axis nano-positioner(FNP) is used in our homemade AFM equipment to get precise nano motions to align the fiber tip over cantilever(See fig.3.7). FNP contains total of six piezo-electric stacks. Three on the base plate and three on the front plate. Each one of these stacks is made of three piezo plates which is placed in specific orientation(see fig.3.9). The orientation of piezo plates are up, down and right piezos in this particular order. Wires are then connected from each piezo junction and the circuit is thus made.

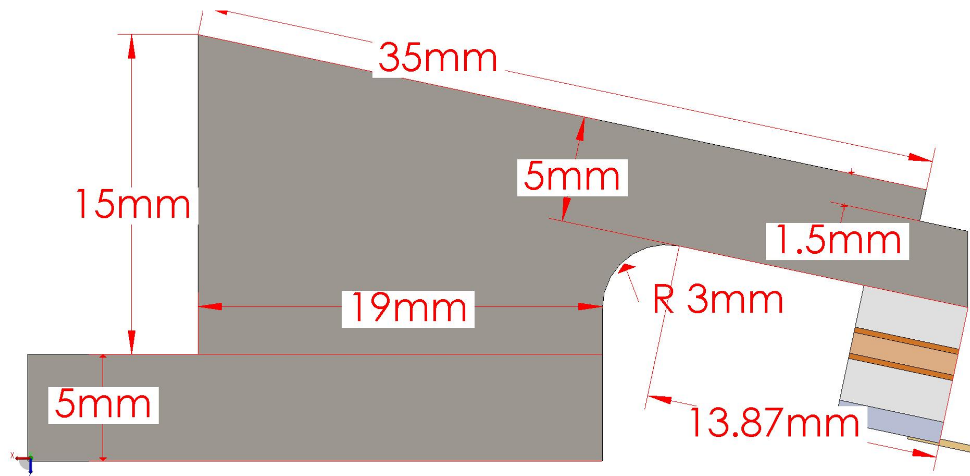

Figure 3.4: Dimensions of Cantilever Holder. Note: The angle between the sides 35mm and 15mm is 12^0

Once we got the stacks in the plate, a small ruby ball is attached to the end of each stack with the help of an insulator(macor). Two such slider plates are placed perpendicularly to achieve the five axis motion(x, y, z, θ, ϕ). They are kept in place with the help of magnets(see fig.3.8).

The ruby balls are allowed to slide over sapphire plates to get sufficient frictional force for inertial motion. As said earlier, the sliders work on the principle of inertial sliding motion[18]. The piezos when applied a voltage pulse will expand in its natural direction, taking along with it the attached object. And when the voltage drops to zero, the piezo will contract, but the object will stay in its new position. And on stacking different orientation piezos on top of one another, we get the desired motion.

3.4.3 Sample Movement Assembly

The Sample Movement Assembly comprises three main components: a platform, a scanner-piezo, and a hammer-piezo.

Movement of the sample cell is achieved by the movement of hammer and scanner piezo. The bottom of the sample cell is made of a magnetic steel. A sample platform, containing three magnets(see figure 3.16) which holds the sample cell firm in it place.

The scanner-piezo, shaped cylindrically, is divided into four quadrants on its outer surface, each functioning as an individual electrode, while its inner surface serves as a common electrode for all outer electrodes. During the experiment, pulses are applied to the scanner-piezo to displace

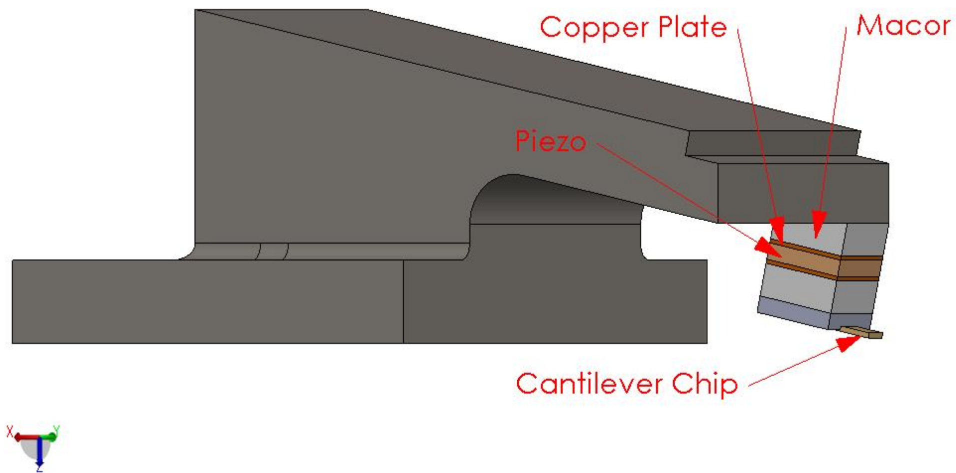

Figure 3.5: Cantilver Holder with its components. Macor(5x5x2), Piezo(5x5x1), Cantilever Chip, Copper Plates

the sample along all three directions. The hammer-piezo facilitates the coarse adjustment of the sample-stage, bringing the sample closer to the cantilever. This adjustment is achieved by supplying sawtooth pulses to the hammer-piezo, exploiting the inertial effect on motion. Additional details can be found in reference [140].

3.5 Assembly

Figure 3.17, 3.18 and 3.19 shows the assembly.

3.6 Calibration

3.6.1 Fiber Piezo

Calibration of the fiber piezo can be achieved by defining a k Fiber parameter in the SPM software, denoting the fiber extension or retraction per given unit voltage.

The calibration procedure:

1. Aign the two mirrors exactly parallel to each other to capture an interference pattern resulting

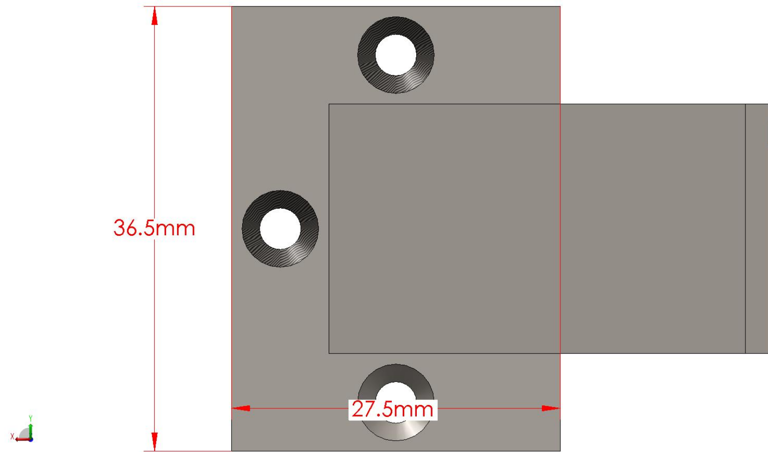

Figure 3.6: Cantilever Holder

from the fiber piezo's back-and-forth movement induced by a known voltage. (Precise alignment is not necessary.)

2. The interference pattern corresponds to the Airy function associated with the Fabry-Perot etalon. It's notable that the consecutive peaks in the Airy function are spaced apart by $\lambda/2$.

3. Employ a Laser diode with a wavelength of 1310 nm as the light source. Consequently, the gap between two peaks of the plots Airy functions should be 655 nm. By observing the interference pattern output and ensuring the spacing between peaks, the k-fiber parameter in Å/mV can be adjusted accordingly.

4. The k-fiber parameter varies based on the dimensions and sensitivity of the fiber piezo and should thus be recalibrated whenever there are alterations to the piezo or soldering. In the current setup, the k fiber constant is set at 127 Å/mV.

3.6.2 Scanner Piezo

Scanner Z calibration involves accurately calibrating the movement of the scanner piezo in the Z dimension, as parameters such as extension and pulling speed are influenced by the displacement of scanner Z.

This calibration process is conducted as:

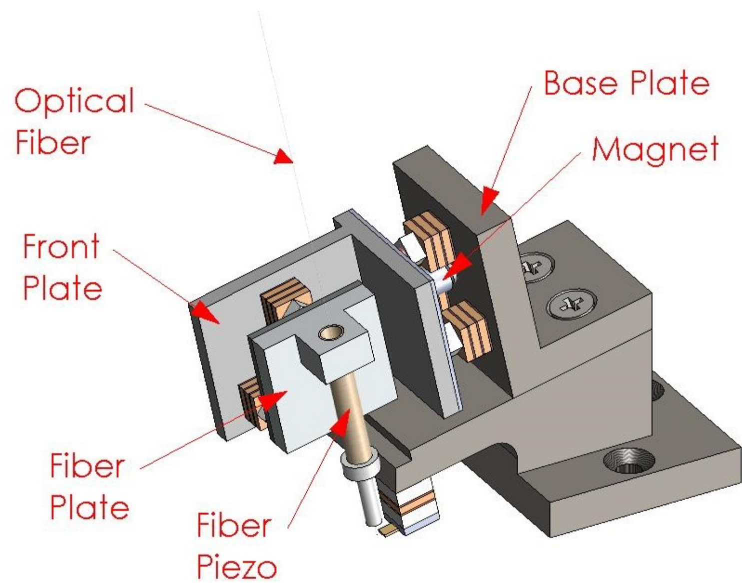

Figure 3.7: Five Axis Nanopositioner along with cantilever holder assembly

1. Align the two mirrors exactly parallel to each other.

2. Halt the movement of the fiber piezo, hence intensity pattern for constant intensity is displayed.

3. Apply a predetermined voltage to the scanner to initiate motion in the Z-axis (ensuring voltage on each face is same.) Document the consistent intensity registered on the photodiode for each applied voltage.

4. Graph the intensity values recorded against the applied voltage. This graph should replicate the interference pattern, depicting the movement induced by the scanner's piezo component.

5. Using a method akin to the one described earlier, we calculated the calibration factor, defined as the displacement per applied voltage, denoted in nm/V. In our configuration, this value was determined to be 18 nm/V.

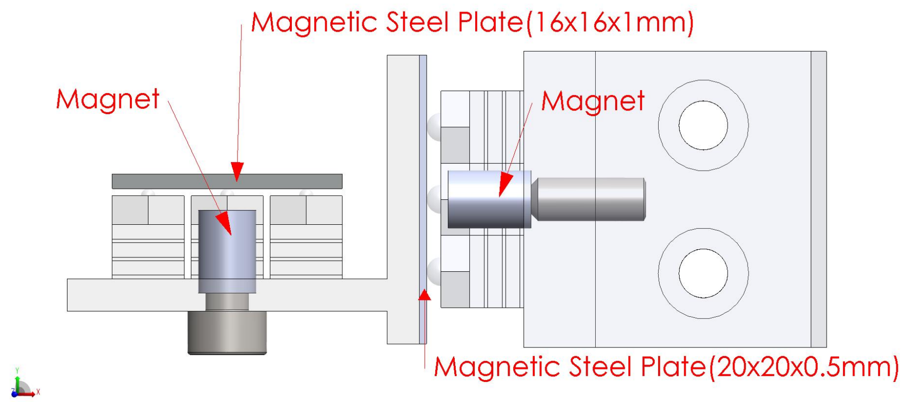

Figure 3.8: Depiction of magnets holding the front and fiber plate. Thin sapphire glass sheets are glued on magneic steel plates where ruby balls touches the magnetic steel plate. Note that magnets are not touching the magnetic plates. This ensures that plates are only touching the ruby balls.

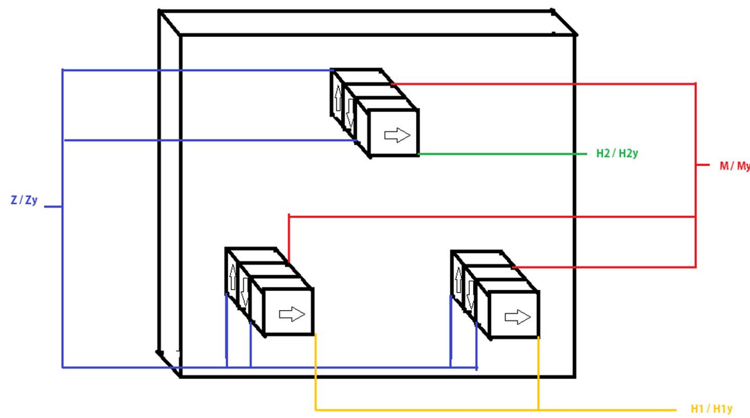

Figure 3.9: Directions of piezo movements and wlwctrical connections. Connections Z, H2, M, H1 correspond to base plate whereas, connections Zy, H2y, My, H1y correspond to front plate.

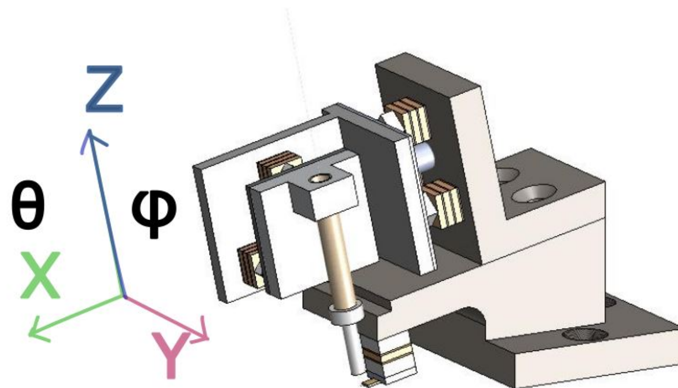

Figure 3.10: The X, Y, and Z axes

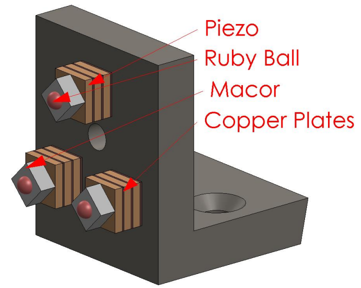

Figure 3.11: The Base Plate

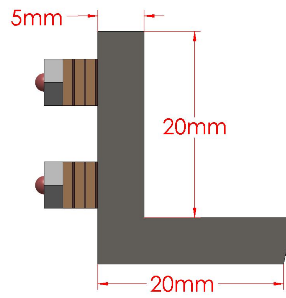

Figure 3.12: The Base Plate

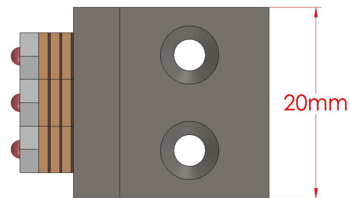

Figure 3.13: The Base Plate

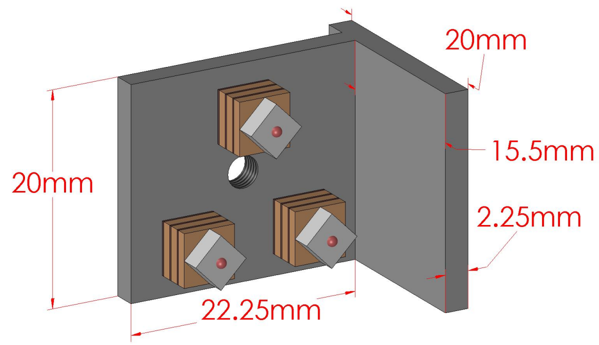

Figure 3.14: The Front Plate

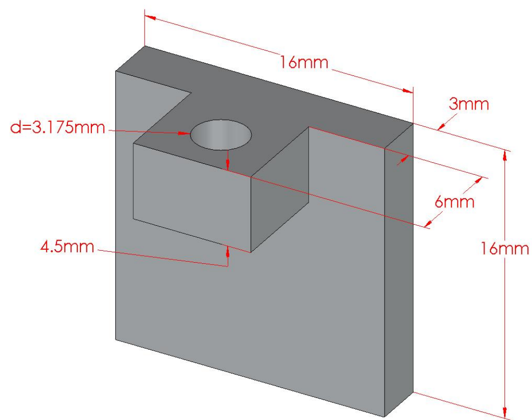

Figure 3.15: The fiber Plate

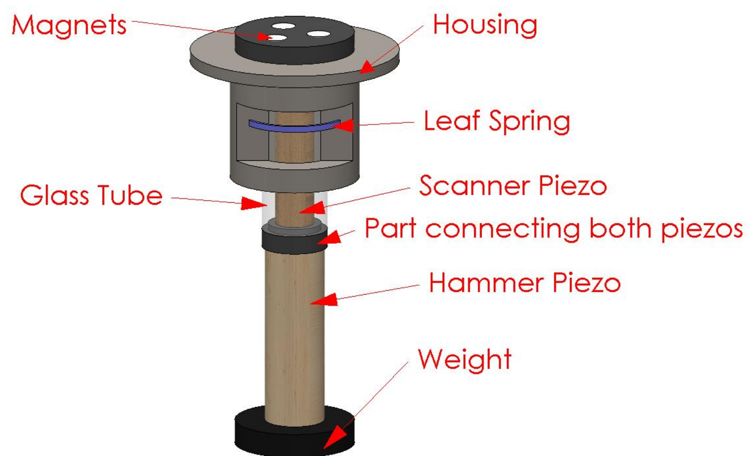

Figure 3.16: The sample movement assemply containing scanner piezo, hammer piezo, leaf spring, etc.

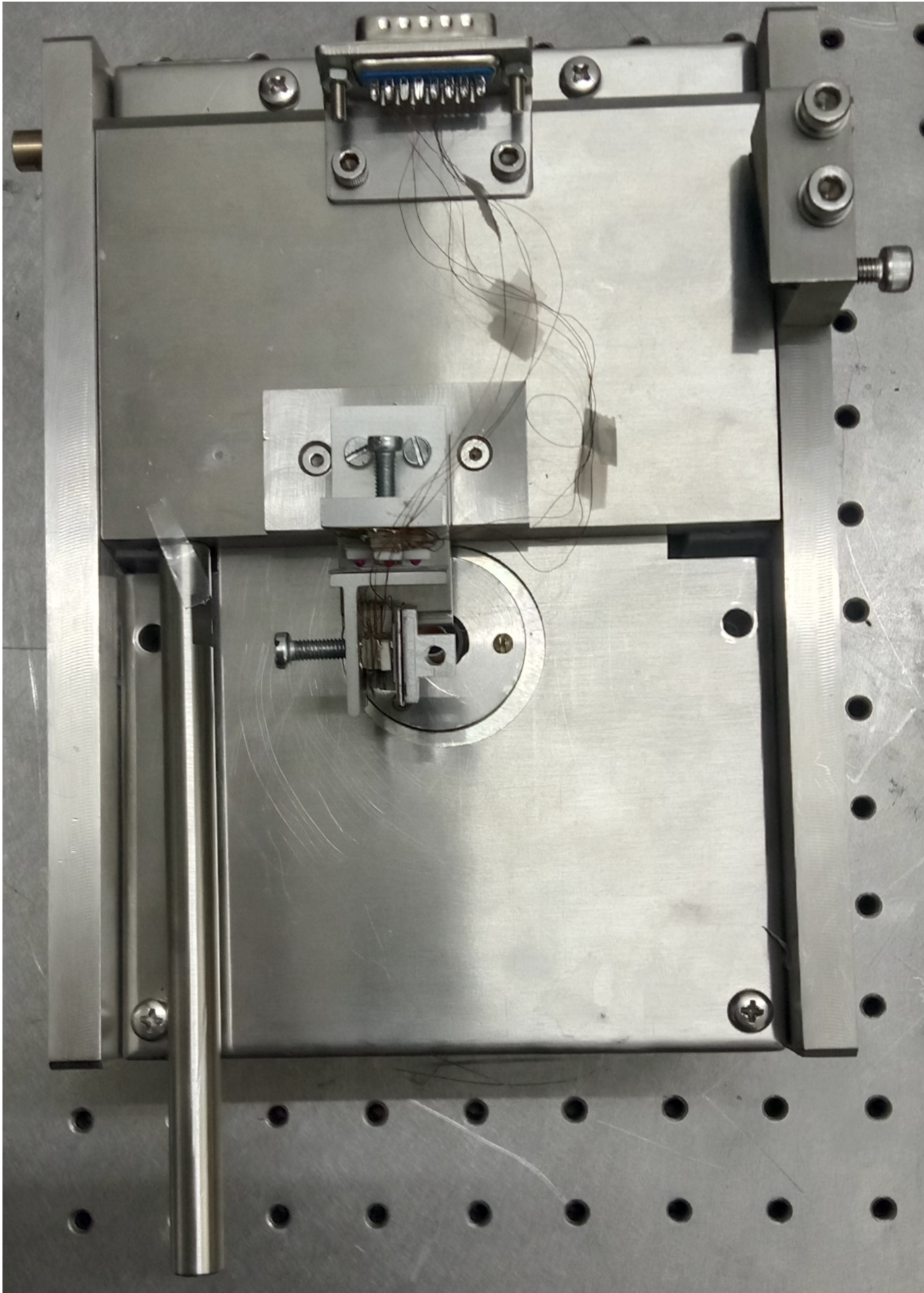

Figure 3.17: Assembly for the interferometer based AFM (view 2)

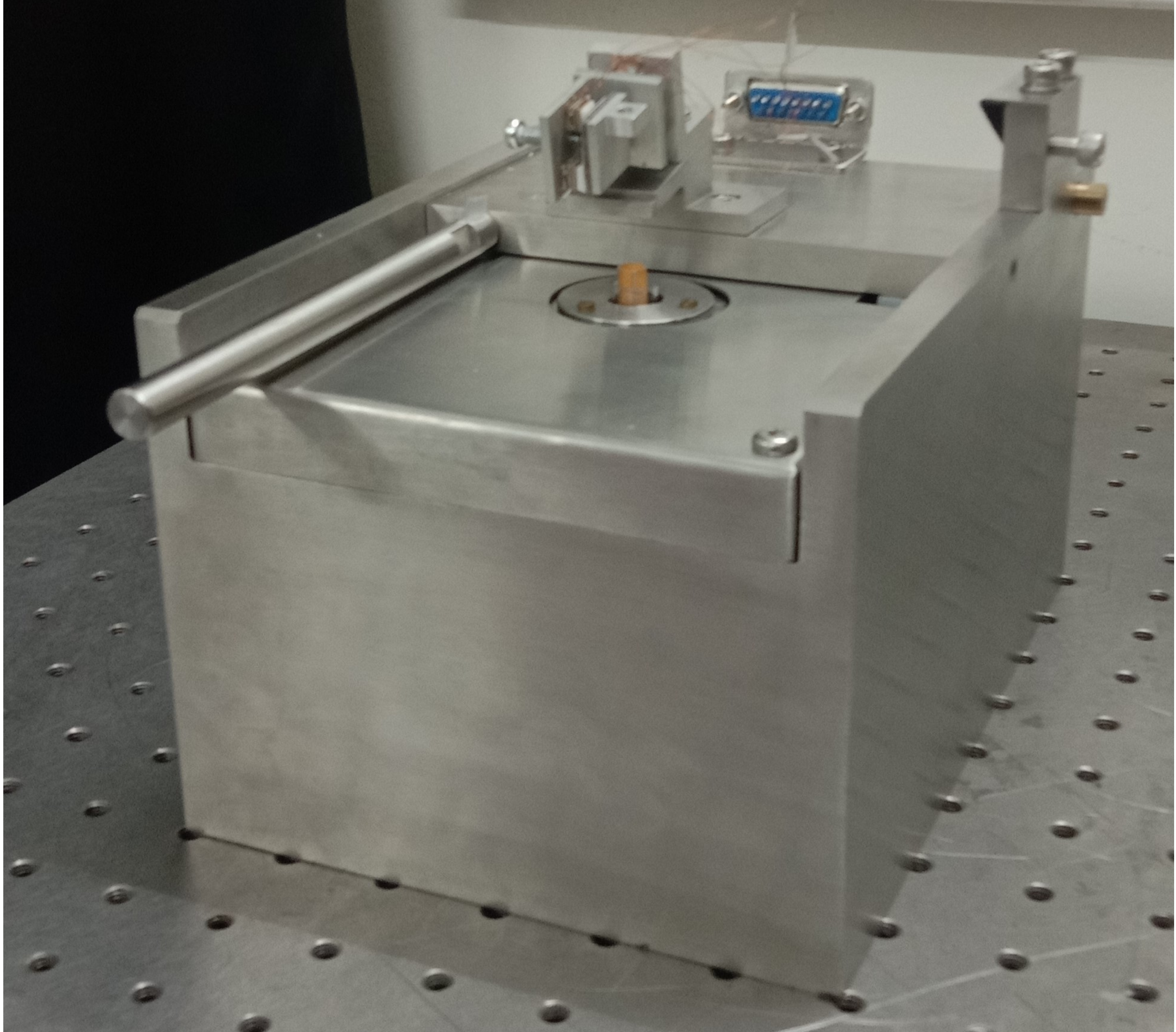

Figure 3.18: Assembly for the interferometer based AFM (view 3)

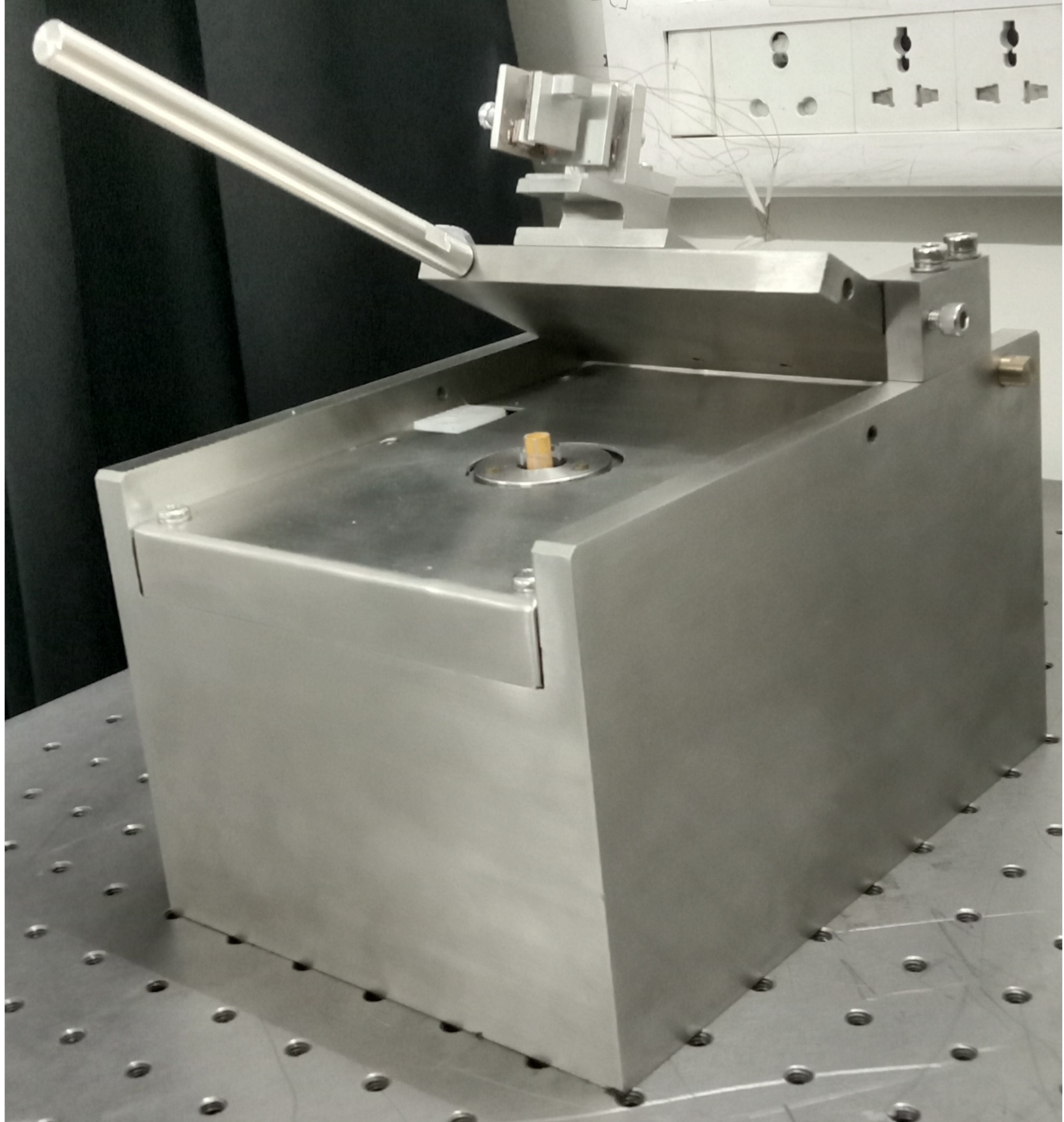

Figure 3.19: Assembly for the interferometer based AFM (view 1)

Chapter 4

Results and Discussion

After assembling the instrument, we check for the stability of the instrument.

4.1 Optical fiber and the cantilever

The distance between optical fiber and the cantilver can be monitored by monitoring the fiber piezo voltage. The fiber is locked at the distance with maximum sensitivity of the interferometer. If the distance between the two mirrors changes, then, to maintain the high sensitivity, the fiber piezo is given a voltage automatically throuh computer programme to retract or approach and hence maintains the constant distance. So, by plotting the fiber piezo voltage Vs time, we can get an idea of the drift.

Figure 4.1 consists of plots of Fiber piezo voltage Vs time for five experiments. From section 3.6.1, we can calculate the drift between the optical fiber and the cantilever for 50 minutes.

- Experiment 1: 292.672 nm
- Experiment 2: 467.059 nm
- Experiment 3: 192.000 nm
- Experiment 4: 94.093 nm

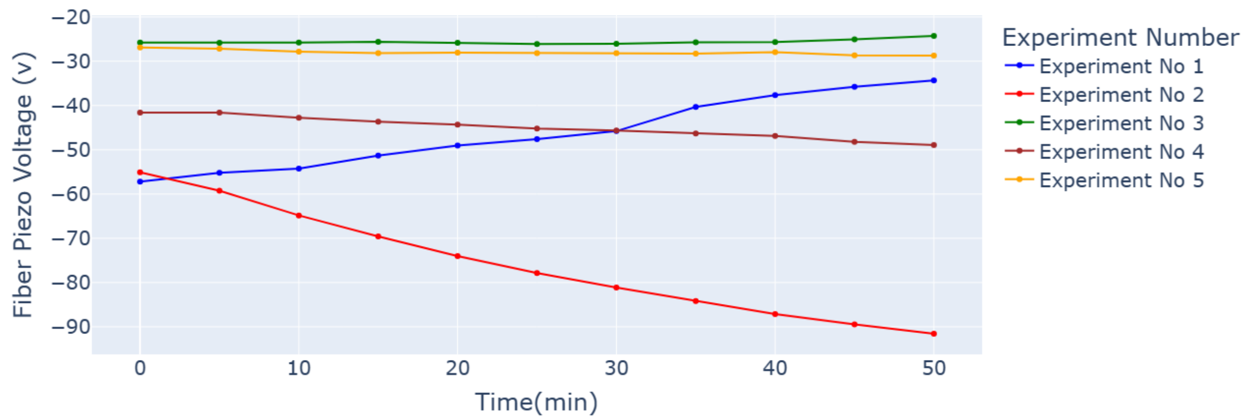

Figure 4.1: Fiber piezo voltage (V) Vs Time (min) for the five experiments performed. The changes in fiber piezo voltage indicate the drift between the end of the optical fiber and the cantilever. The drift between optical fiber and cantilever is found to be: Experiment 1: 292.672 nm, Experiment 2: 467.059 nm, Experiment 3: 192.000 nm, Experiment 4: 94.093 nm, Experiment 5: 23.232 nm

- Experiment 5: 23.232 nm

4.2 Cantilever and the substrate

When the substrate is approached, it is locked for a given amplitude of the tip. If the distance between the cantilever and the sbstrate changes, the computer programme automatically adjusts the scanner piezo voltage and the distance between them is kept constant. So, by plotting z voltage as function of time can give us idea of the drift.

Figure 4.2 consists of plots of Fiber piezo voltage Vs time for five experiments. From section 3.6.2, we can calculate the drift between the cantilever and the substrate for 50 minutes.

- Experiment 1: 4.878 nm
- Experiment 2 14.202 nm
- Experiment 3: 1.206 nm
- Experiment 4: 2.772 nm

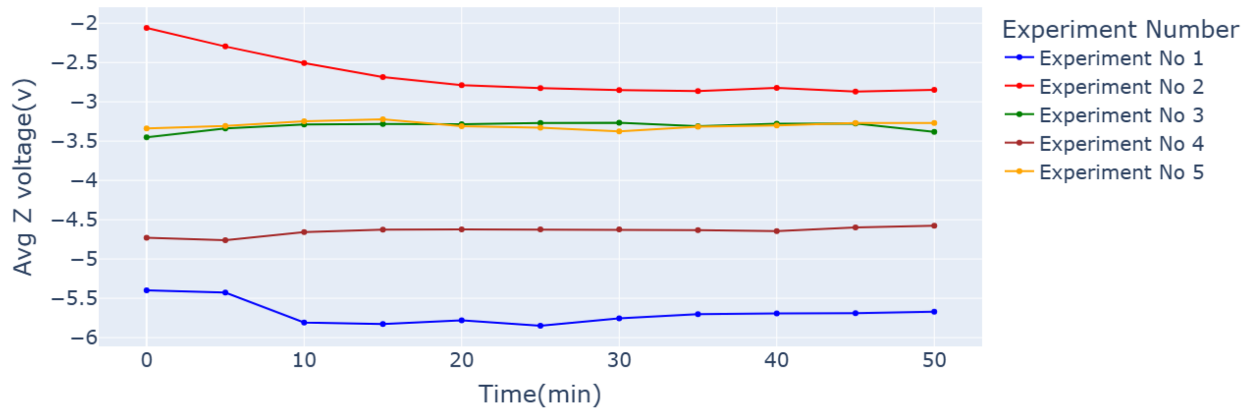

Figure 4.2: Avg Z voltage (V) (given to scanner piezo) Vs Time (min) for the five experiments performed. The changes in Z voltage indicate the drift between cantilever and the substrate. The drift between the cantilever and the substrate for 50 minutes was found to be: Experiment 1: 4.878 nm, Experiment 2 14.202 nm, Experiment 3: 1.206 nm, Experiment 4: 2.772 nm, Experiment 5: 1.242 nm

- Experiment 5: 1.242 nm

4.3 Discussion

From section 4.1 and section 4.2 we can clearly see the drift. However, the drift has been reduced more or less as we do more experiments. This is because, after first experiment we ralised that the magnets holding the five axis nano positioner may not be holding it tightly, so we brought the magnet closer to the steel plates. We are investigating the way to reduce the drift and improving the stability.

Chapter 5

Future Plans

We are planing to do a force measurements for I1 domain of titin protein along with I27 domain of titin and then compare the force vs extension plots to observe difference of visco-elasticity of I1 and I27.

In I27 we are hoping to see a hump region in force vs extension plot which will correspond to the intermediate state of the unfolding I27 domain. Whereas, in case of I1, we are expecting no hump region in force extension plot which will clarify that I1 has no unfolding intermediate.

This will be a novel way to measure viscoelastic property of complex biological molecules like proteins with more accuracy by using interferometer based atomic force microscope.

Bibliography

[1] TR Albrecht, S Akamine, TE Carver, and CF Quate. Microfabrication of cantilever styli for the atomic force microscope. *Journal of Vacuum Science & Technology A: Vacuum, Surfaces, and Films*, 8(4):3386–3396, 1990.

[2] H Becker, O Bender, L Bergmann, K Rost, and A Zobel. Apparatus for measuring surface irregularities, 1955.

[3] Fabrizio Benedetti, Yulia Gazizova, Andrzej J Kulik, Piotr E Marszalek, Dmitry V Klinov, Giovanni Dietler, and Sergey K Sekatskii. Can dissipative properties of single molecules be extracted from a force spectroscopy experiment? *Biophysical journal*, 111(6):1163–1172, 2016.

[4] G Binnig. Atomic force microscope and method for imaging surfaces with atomic resolution., 1998.

[5] Gerd Binnig, Calvin F Quate, and Ch Gerber. Atomic force microscope. *Physical review letters*, 56(9):930, 1986.

[6] Gerd Binnig, Heinrich Rohrer, Ch Gerber, and Edmund Weibel. Surface studies by scanning tunneling microscopy. *Physical review letters*, 49(1):57, 1982.

[7] Gerd Binnig, Heinrich Rohrer, Ch Gerber, and Eduard Weibel. $7\times$ 7 reconstruction on si (111) resolved in real space. *Physical review letters*, 50(2):120, 1983.

[8] Surya Pratap S Deopa and Shivprasad Patil. Viscoelasticity of single folded proteins using dynamic atomic force microscopy. *Soft Matter*, 19(23):4188–4203, 2023.

[9] Peter Eaton and Paul West. *Atomic Force Microscopy*. Oxford University Press, 2010.

[10] Ricardo García. *Amplitude modulation atomic force microscopy*. John Wiley & Sons, 2011.

[11] Franz J Giessibl. High-speed force sensor for force microscopy and profilometry utilizing a quartz tuning fork. *Applied physics letters*, 73(26):3956–3958, 1998.

[12] Th Göddenhenrich, H Lemke, U Hartmann, and C Heiden. Force microscope with capacitive displacement detection. *Journal of Vacuum Science & Technology A: Vacuum, Surfaces, and Films*, 8(1):383–387, 1990.

[13] Yves Martin, Clayton C Williams, and H Kumar Wickramasinghe. Atomic force microscope–force mapping and profiling on a sub 100-å scale. *Journal of applied Physics*, 61(10):4723–4729, 1987.

[14] Shuhei Nishida, Dai Kobayashi, Takeo Sakurada, Tomonori Nakazawa, Yasuo Hoshi, and Hideki Kawakatsu. Photothermal excitation and laser doppler velocimetry of higher cantilever vibration modes for dynamic atomic force microscopy in liquid. *Review of scientific instruments*, 79(12), 2008.

[15] Shivprasad Patil, George Matei, Hang Dong, Peter M Hoffmann, Mustafa Karaköse, and Ahmet Oral. A highly sensitive atomic force microscope for linear measurements of molecular forces in liquids. *Review of Scientific Instruments*, 76(10), 2005.

[16] Shatruhan Singh Rajput, Surya Pratap S Deopa, VJ Ajith, Sukrut C Kamerkar, and Shivprasad Patil. Validity of point-mass model in off-resonance dynamic atomic force microscopy. *Nanotechnology*, 32(40):405702, 2021.

[17] Shatruhan Singh Rajput, Surya Pratap S Deopa, Jyoti Yadav, Vikhyaat Ahlawat, Saurabh Talele, and Shivprasad Patil. The nano-scale viscoelasticity using atomic force microscopy in liquid environment. *Nanotechnology*, 32(8):085103, 2020.

[18] Ch Renner, Ph Niedermann, AD Kent, and O/ Fischer. A vertical piezoelectric inertial slider. *Review of scientific instruments*, 61(3):965–967, 1990.

[19] Daniel Rugar, H Jonathon Mamin, and Peter Guethner. Improved fiber-optic interferometer for atomic force microscopy. *Applied Physics Letters*, 55(25):2588–2590, 1989.

[20] G Schmalz. Uber glatte und ebenheit als physikalisches und physiologishes problem. *Verein Deutscher Ingenieure*, pages 1461–67, 1929.

[21] Russell Young, John Ward, and Fredric Scire. The topografiner: an instrument for measuring surface microtopography. *Review of Scientific Instruments*, 43(7):999–1011, 1972.